Advanced combustion modelling of high bmep engines under water injection conditions with chemical correlations generated with detailed kinetics and machine learning algorithms

Advanced Combustion Modelling of High BMEP Engines under Water Injection Conditions with Chemical Correlations Generated with Detailed Kinetics and Machine Learning Algorithms

Author, co-author (Do NOT enter this information. It will be pulled from participant tab in MyTechZone)

Affiliation (Do NOT enter this information. It will be pulled from participant tab in MyTechZone)

Abstract

Water injection is becoming a technology of increasing interest for SI engines development to comply with current and prospective regulations. To perform a rapid optimization of the main parameters involved by the water injection process, it is necessary to have reliable CFD methodologies capable of capturing the most important phenomena. In the present work, a methodology for the CFD simulation of combustion cycles of SI GDI turbocharged engines under water injection operation is proposed. The ECFM-3Z model adopted for combustion and knock simulations takes advantages by the adoption of correlations for the laminar flame speed, flame thickness and ignition delay times prediction obtained by a detailed chemistry calculation. The latter uses machine learning algorithms to reduce the time to generate the full database while still maintaining an even distribution along the variables of interest. The results demonstrate the applicability of the proposed methodology, capable of capturing not only the thermodynamic effects of water injection but also the chemical kinetics aspects related to the mixture water dilution whose prediction is mandatory for addressing the engine design according to different goals: complying with new emission directives and limits, turbine inlet temperature constraints, minimization of the BSFC and possibly engine power increase.

Introduction

Currently the application of fuel enrichment strategy for component protection (i.e., Turbine Inlet Temperature control) results in a dramatic increase of raw emissions, especially CO emissions, because they cannot be handled by the three ways catalyst (TWC). In the coming future the development of S.I. engines operating at lambda 1.0 in the overall map is recommended. The most demanding points are those close to full power since the exhaust gas temperature at turbine inlet (TiT) may increase above the limits because of the lack of fuel cooling effect. In this scenario, the water injection is one of the exploited technologies, together with the use of overexpansion cycle (Miller or Atkinson), cooled EGR, improved turbocharge, ignition system technology and alternative fuels. It must be considered that the injection of water changes both the thermodynamic and the chemical behavior of the mixture. If the thermodynamic effects can be currently well captured with standard RANS CFD simulations, the effects of the water dilution on combustion duration, and indirectly also on the TiT and the engine knock limit, ask for the accurate prediction of the flame laminar speed, the flame laminar thickness and the auto-ignition time. In fact, if the main positive aspect of the water injection is its strong mixture cooling capability, besides it, it is well known that the water vapor acts as a mixture diluter, thus diminishing the reactants burning rate and changing the auto-ignition delay time [1-4]. Before entering the actual topic of scientific work, a brief analysis of the literature is necessary. Many authors have studied the effect of the water injection on the combustion efficiency [5-12] and, for brevity's sake, here some scientific works only have been cited and commented. In the field of the experimental research, it has to be cited the work by Gern [13], where the influence of water injection on the combustion process and raw emissions was experimentally analyzed on a single-cylinder research engine with direct and indirect water injection. The authors highlighted that, even though water injection initially slows down the combustion process, both injection concepts allow shifting the knock limit and reducing the exhaust gas temperature. In [14] Vacca et al. aimed to the comprehension of multiple thermodynamic effects related to water injection and to the enhancement of combustion efficiency through 3D-CFD simulations. Finally, very interesting for the present research is the work by Fandakovet al. [15] where they extended the work presented in 2017 [16] with the inclusion of water: they presented a detailed reaction kinetics mechanism focused on the prediction of the low- and high-temperature mixture ignition stages (two-stage ignition) and of the temperature increase resulting from the low-temperature ignition. From an engineering point of view, the accurate (not easy) prediction of the thermodynamics and physical effects of liquid and vapor water is not sufficient since the trade-off between combustion duration, knock tendency and TiT ask for complex chemistry. In RANS CFD combustion simulation a very good and effective mean to deal with this requirement is to use combustion models based on the flamelet approach (i.e. ECFM-3Z, G-Equation models) which accounts for both the detailed air-fuel chemistry and the flame-turbulence interaction assuming that the turbulent flame front can be regarded as an aggregate of smaller laminar flames [17].
Depending on the chosen model, the effects of turbulence are accounted for by computing the turbulent flame speed (level set models [18]), or by defining auxiliary variables to describe the corrugated flame front, such as the flame surface density (CFM models [19]). In both approaches, however, the description of the chemical kinetics properties of the mixture is summarized by the unstretched laminar flame speed and thickness. The definition of these quantities has relied for several years on well-established correlations derived from experimental data [20]. The main limitation of this approach is the limited range of the validation domain, which

is usually very far from the conditions reached during the operations of modern engines, and the lack of flexibility with respect to the mixture formulation. To overcome these limitations, in recent years researches have relied more heavily on detailed chemical kinetics simulations of laminar flames [21] to populate look-up tables or generate enough data to fit new correlations. The same approach can be applied also for the description of the ignition delay time of the reacting mixture, for which similar limitations are present.
Despite being widely recognized as a viable approach [22], the use of detailed chemical simulations for the generation of a laminar flame speed database is extremely time consuming when adopting complete chemical kinetics schemes.
Since the fuel considered may change from application to application and in next future (different gasoline blending, biofuels, e-fuels), and since in many cases more than one fuel surrogate and more than one chemistry scheme are tested, it comes out that the detailed chemistry solver-based calculations used to build-up look up table or correlations may require an unfeasible time, also using strong HPC resources.
The aim of this research activity is to define and validate an end to end methodology based on chemical kinetics reduction and machine learning algorithms for the definition of the reaction properties needed for the CFD simulation of internal combustion engines also in the presence of water vapor. This approach relies on the previous one by Pulga et al. [22, 23].
The correlations deriving from the above datasets have been applied to the RANS-CFD combustion simulations by using the CFD solver Fire v.2014 by AVL of a Proof-of-concept GDI engine, virtually designed at the University of Bologna, following the actual and future market guidelines with emphasis on showing how the detailed chemistry can help in addressing parameters trade-off.

The research activity has been presented in this paper splitting the main items in the following paragraphs:

1. Engine specifications.
2. Simulation setup.
3. Machine Learning methodology.
4. Water injection system and engine configurations: non-reacting flow results.
5. Water injection system and engine configurations: reacting flow results.

THE ENGINE SPECIFICATIONS

A high-bmep and high-power S.I. GDI turbo-charged engine has been virtually designed at the University of Bologna and slightly modified compared to the previous one [2]. In Figure 1 the engine is visible, in the DWI version in Figure 1a and in the PWI configuration in Figure 1b, respectively, with the same compression ratio for both. The water injector spray targeting was carefully chosen in both configurations to minimize the wall impingement, especially on the piston periphery, and therefore to promote the water evaporation within the airstream and from the liquid film formed on walls. The injector in the DWI case is mounted on the intake side of the engine head. This helps in the overall drawing of the engine head and it allows larger free spray path between the injector and the cylinder or piston surfaces. Moreover, the water spray beam orientation was set to promote the interaction between the water plumes and the in-cylinder air-flow field, enhancing the water evaporation rate. The injector characteristics have been resumed in Table 1. The fuel injector is centrally located with a spray targeted to spark plug for promoting combustion during cat-heating phase. Table 2 resumes the main specifications of the adopted high-bmep engine. The operating point considers the full power condition listed in Table 3.

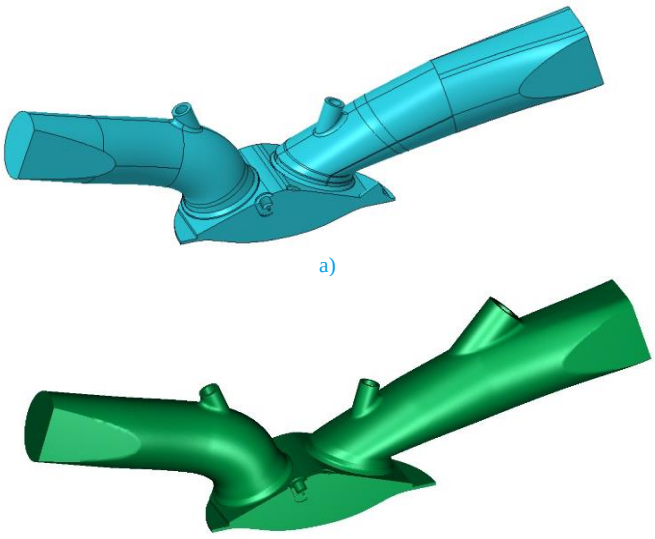

a)

b)

Figure 1. Virtual engine with a) DWI system; b) PWI system

Table 1. Gasoline and water injector characteristics

	GASOLINE	DWI	PWI
Number of holes [-]	8.0	5.0	2.0
Injection pressure [bar]	350.0	50.0/150.0	10.0
Injection temperature [K]	313.0	313.0	313.0
HFR [cm^3/s]	20.0	17.0	17.0
Hole geometric diameter [µm]	188.0	220.0	347.0

Table 2. Main characteristics of the engine

Unit Displacement [cm^3]	471.05
Stroke S [mm]	85.00
Bore D [mm]	84.00
Conrod length [mm]	165.60
Number of valves	4.00
S/D [-]	1.01
Intake D_V/D [-]	0.36
Exhaust D_V/D [-]	0.33
Compression ratios	9.50:1.00 / 10.50:1.00
Squish Height [mm]	1.10

THE SIMULATION SETUP

The boundary and the initial conditions for the CFD simulation at the considered operating point have been derived by running a one-dimensional simulation using the open source code OpenWAM. The

engine cycle three-dimensional CFD simulations, whose setup is shown in Table 4, were performed following a multi-cycle approach: the presented results refer to the last converged engine cycle. Differencing schemes are second order for mass, momentum and energy, while turbulence is resolved with a second order blended scheme. The solution is converged when the residual error for each equation is below the tolerance threshold of 1e-4. Non-reacting flow simulations and reacting flow simulations have been performed. Non-reacting flow simulations have been stopped at TDC of the converged cycle and they are aimed to assess the behavior of water injection system and operating conditions. Combustion system half-geometry domain has been considered because of the symmetry conditions. The computational mesh has 506.000 cells at TDC.

Table 3. Engine operation point at full power

Engine speed [rpm]	7000.0
Engine load	100.0%
Spark Advance	Sweep until knock limited
Mixture index (w/o water) [-]	1.0
Boost pressure [bar]	2.7
Max BMEP [bar]	26.6
Inlet valve opening [CA deg. ATDC]	362.0
Inlet valve closing [CA deg. ATDC]	598.0
Exhaust valve opening [CA deg. ATDC]	136.0
Exhaust valve closing [CA deg. ATDC]	376.0

Table 4. Main settings for CFD simulations

Start angle	330 CA deg. ATDC
End angle	856 CA deg. ATDC – corresponding to EVO
Turbulence model	K-z-f
Wall heat model	Hybrid wall treatment
Law of the wall	Standard + Han-Reitz
Evaporation model	Spalding
Wallfilm evaporation model	Combined
Wallfilm entrainment model	Schadel - Hanratty
Wallfilm splashing model	Kuhnke
Atomization model	Slightly modified version of the model presented in [6]
Breakup model	
Combustion model	ECFM-3Z adopting correlations for LFS, flame thickness and auto-ignition delay time
Ignition model	Lagrangian ignition model [18, 19]
Knock model	Two steps autoignition model based on [21]

The parameter s has been adopted to measure the injected water mass per cycle and cylinder, and it is defined as the ratio between the injected water mass and the stoichiometric fuel mass of the given engine operation point. Relative humidity of the intake air has been considered.

MACHINE LEARNING METHODOLOGY

Methodology focused on the laminar flame property derivation

For the calculation of the laminar flame speed and thickness, the methodology proposed in the work by Cazzoli et al. [21] was followed by performing the iterative solution with grid refinement of a steady adiabatic free flame in a 1D domain. The length of the domain for each simulation was chosen iteratively by assuming an initial value of 3e-3 m and reduced in order to converge to a solution not affected by the ignition chemistry as described in [24]. The code was implemented in Python [25] leveraging the Cantera library [26]. Considering the properties of planar unstrained flames, the laminar flame speed is defined as the displacement speed of the unburnt mixture, while the flame thickness is computed from the temperature profile along the propagation direction [17] as described in Eq. 1.

$$\delta_L{}^0 = \frac{T_2 - T_1}{max\left(\left|\frac{dT}{dx}\right|\right)} \qquad (1)$$

As reported in [23], the use of the laminar flame speed obtained from detailed chemical kinetics simulations allows for the definition of a consistent value of laminar flame thickness by following the relation proposed by Blint [17], with a scaling factor equal to 0.626. In Eq. 2 subscript 1 indicates the property of the fresh mixture, while 2 indicates the properties of the burnt mixture, λ is the thermal conductivity, C_P the specific heat, ρ the gas density and S_l the laminar flame speed.

$$\delta_L{}^{Blint} = 0.626 \cdot \left(\frac{\lambda}{\rho C_P S_l}\right)_1 \cdot \frac{(\lambda/C_P)_2}{(\lambda/C_P)_1} \qquad (2)$$

The chosen fuel is the TAE7000 [27], with RON=98.1 which was experimentally compared in terms of laminar flame speed to a TOTAL commercial gasoline and for which an appropriate surrogate was defined (composition: 13.7% (vol.) n-heptane NC7H16, 42.9% iso-octane IC8H18, 43.4% (vol.) toluene C7H8). The dataset of LFS values should represent all the possible combinations of pressure (P), temperature of the unburnt mixture (T_u), equivalence ratio (ϕ) and the diluent fractions distinguished between exhaust gas recirculation (X_{EGR}) and pure water vapor (X_{H_2O}) with a sufficiently small discretization step, as proposed in Table 5.

Table 5. Grid points for LFS simulations

	Min/max	# points
P (bar)	5 – 160	7
T_u (K)	450 – 1100	14
ϕ (-)	0.3 – 2.5	16
X_{EGR} (%)	0 – 30	5
X_{H_2O} (%)	0 – 6	4

The total number of simulated points is higher than 30000 and, even if the combinations of pressure and temperature that would not be reached inside the combustion chambers were removed (i.e. high pressure and low temperature and vice-versa), the number would be reduced by at most 25%. By using the validated chemical kinetics mechanism proposed by the Polimi CRECK group [28] on a computer with CPU Intel Xeon Platinum at 3.0 GHz, with 144 GB ram, Cantera version 2.3.0 and Python version 3.7.2, on average one simulation requires about 1000 seconds per point to converge, which means more than 8500 CPUh's for the full dataset. In order to reduce the time required to populate the dataset, the chemical kinetics mechanism can be reduced by applying an automatic reduction methodology defined as DRGEP (directed relation graph with error propagation) [29] with Sensitivity Analysis [30], implemented in the Python package PyMARS [31]. By applying this method, a series of ignition simulations is performed and the relation between different species is represented in a graph structure where the nodes indicate the species and the thickness of the edges is the interaction coefficient between species. After the computation, a cutoff threshold is used to remove the less relevant interactions and therefore the vertices that are no-longer connected with the target species. After this step, the sensitivity analysis performs an evaluation of the error induced by the removal of each single species on the ignition computation. This approach would require a significant amount of computing time, and it is therefore applied subsequently to the DRGEP only on the species that would have been removed if the cutoff threshold were higher (but still within a given value, set to 0.4 for this application). The resulting scheme is adopted to evaluate the relative error performed on a series of zero dimensional simulations at given pressure, temperature and mixture composition that represent engine relevant conditions. Considering a threshold value for the sensitivity analysis of 0.4, and an admissible relative error of up to 70%, by using the TAE surrogate components and N_2 , O_2 as target species, the resulting mechanism is the 'red_140' whose features are reported in Table 6.

Table 6. Features of the complete and reduced mechanisms

SCHEME	# SPECIES	# REACTIONS	CPUh
POLIMI	352	9705	1000 s
red_140	140	3030	100 s

Considering the nature of the problem, a rough estimate of the computing time for chemical kinetics simulations is that it scales quadratically with the number of species, therefore the CPU hours needed for a single simulation with the reduced scheme are aligned with the expectations. The validations of the POLIMI chemical kinetics scheme and of the reduced mechanism have been performed by comparing the values of laminar flame speed with experimental data available from [27], for the adopted surrogate at 358 K and 1 bar. As it can be noticed in Figure 2, for lean mixtures the results of both mechanisms show a good agreement with the experimental data, but the reduced mechanism overestimates the LFS for stoichiometric to rich mixtures. In order to generate a full dataset of reference points with the same accuracy level of the full mechanism but the computing time of the reduced scheme, a methodology has been applied for the recovery of the accuracy level of a grid generated with the red_140 scheme.

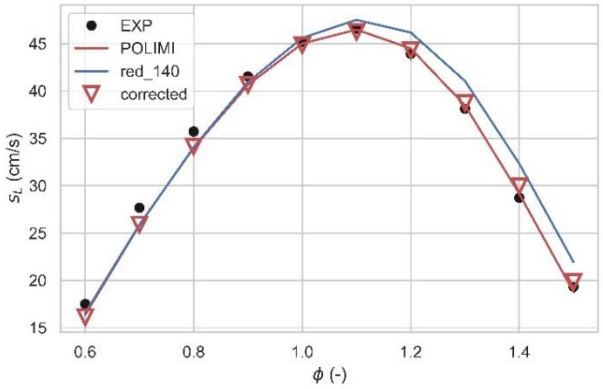

Figure 2. LFS for TAE7000 surrogate at T=358 K, P=1 bar

The idea behind the approach followed in the present work was demonstrated in [22], whose aim is to generate the full table with the reduced mechanism and train a regression model to predict the correction term (η) for combining the speed of calculation of the reduced scheme with the accuracy of the results of the detailed one, as reported in Eq. 3.

$$\widetilde{s_L} = (s_L)_{1D\_red} \cdot (1 + \eta_{ML}) \qquad (3)$$

In Eq. 3 $\widetilde{s_L}$ is the corrected value of LFS, $(s_L)_{1D\_red}$ is the value tabulated with the reduced chemical kinetic mechanism, and η_{ML} is the corrective factor predicted by the machine learning algorithm for each point. Considering the fact that the reduced mechanism employed is not the same reported in [22], a validation of the methodology has been performed on a split of the available dataset. The metrics used to evaluate the performance are RMSE (Root Mean Square Error, the square root of the mean squared difference between target and predicted values) and R2 (determination coefficient) which is calculated in its general form as in Eq. 4, where y_i represents the target value, $\bar{y}$ indicates the mean of the available data, and f_i is the target value predicted by the algorithm:

$$R^2 = 1 - \frac{\sum_i (y_i - f_i)^2}{\sum_i (y_i - \bar{y})^2} \qquad (4)$$

After generating a reduced version of the dataset of LFS, consisting of about 3% of the points of the full grid with both POLIMI and red_140 schemes, the target variable η_{ML} has been defined by inverting Eq. 3. The hyperparameters of the regression model AdaBoost [32], which was found in [22] to provide the best performance in terms of accuracy for small datasets, have been optimized on 70% of the reduced dataset and the performance evaluated on the remaining 30% using the implementation of the algorithm available in the library Scikit-Learn [33]. The results on the train set show a RMSE=0.003 and R2>0.999, while for the test set the RMSE=0.007 and R2>0.998, with errors localized mainly for values of ϕ smaller than 0.4 or greater than 2.5. After applying the correction term, the laminar flame speed with the reduced mechanism of the test set has been compared with the reference values before and after the correction, the relative error distribution has been reported in Figure 3. The error distribution shows that the correction process has reduced the mean error values and its standard deviation significantly, in fact 98% of the points in the test set have an absolute relative error lower than 1.8%.

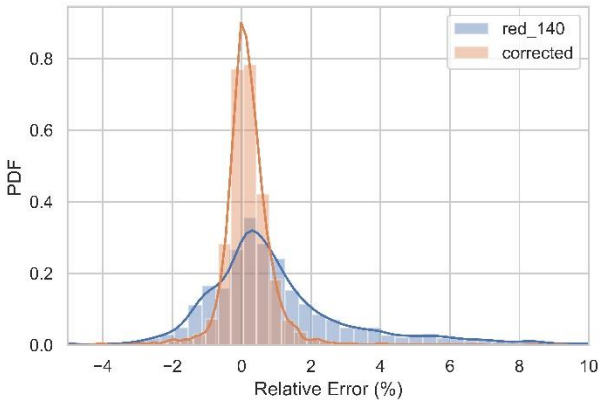

Figure 3. Relative error performed by the reduced mechanism before and after the correction step on the test set

In order to further reduce the chemical kinetics simulations necessary for the generation of the full dataset, a different machine learning approach has been adopted to synthetically increase the number of reference points with respect to the water mass fraction. The hybrid approach adopted would account also for the weaker relations that cannot be captured by traditional correlations. The followed workflow is presented in [23] and consists in assuming a linear correlation for the effect of water addition with a variable coefficient of proportionality predicted by a neural network, as reported in Eq. 5.

$$\widetilde{s_L} = s_{L_0} \cdot \left(1 - k_{ML}\left(P, T_u, \phi, X_{EGR}, X_{H_2O}\right) \cdot X_{H_2O}\right) \qquad (5)$$

$\widetilde{s_L}$ represents the predicted LFS with water effect considered, s_{L_0} is the reference value of LFS at the same operating point but with $X_{H_2O} = 0$, and k_{ML} represents the coefficient of proportionality predicted by a trained regression algorithm as a function of the thermodynamics conditions and the mixture composition. The double presence of the term X_{H_2O} both as the independent variable and as a feature for the regression algorithm is required in order to include the non-linear effect of water addition on LFS. Therefore, after generating the full dataset with X_{H_2O}=0% and a fraction of the dataset (25% of the points for X_{H_2O}=1%, X_{H_2O}=2%, X_{H_2O}=4% and X_{H_2O}=6%), the target variable k_{ML} has been generated by inverting Eq. 5. The neural network was generated using the Keras library [34] and its architecture and hyperparameters have been trained on 70% of the dataset (i.e. about 5000 points) and validated against the remaining 30%. The final neural network consists of 5 nodes in the input layer with tanh activation function, 50 nodes in two hidden layers with ReLu activation function, and one output layer node. The results of the optimized model show for the train set a value of RMSE=0.016 and R2>0.97, while for the test set the RMSE=0.03 and R2>0.95. The adoption of the hybrid method, as demonstrated in [23], allows to avoid the generation of unphysical variations to the LFS when X_{H_2O}=0, since the output of the neural network is directly multiplied by the water mass fraction.

By applying both hybridization methodologies, the time required for the generation of the full dataset of laminar flame speed and thickness has been significantly reduced while maintaining a high level of accuracy, comparable with the results of the complete chemical kinetics scheme. The use of the red_140 mechanism has reduced by 90% the time required to perform the simulations, and the possibility to synthetize grid points accounting for the addition of water vapor has reduced by an additional 50% the computing time. Considering the fact that 3% of the dataset was still generated with the full POLIMI mechanism, the total time to compute the full dataset is reduced by 92%.

After the generation of the dataset, a new correlation has been defined for implementation into the CFD code, optimized on the dataset. Instead of using a classic optimization framework for the definition of the coefficients of the correlation, based on the error committed on the whole dataset, a new objective function has been minimized. The objective function is in the form of Eq. 6.

$$J = 0.7 \cdot |s_l{}^* - s_l|_1 + 0.2 \cdot |s_l{}^* - s_l|_2 + 0.1 \cdot \max\left(|s_l{}^* - s_l|_1\right) \quad (6)$$

Where $s_l{}^*$ represents the LFS predicted by the correlation and s_l is the value obtained with the detailed chemistry simulation. Subscript 1 indicates a region of the database that the engine is more likely to reach during operation, while 2 represents the remaining points. Region 1 has been defined by limiting the values of ϕ between 0.5 and 1.5 and the combinations of P and T_u where the product $P^{1-\gamma} \cdot {T_u}^{\gamma}$ is between 25 and 75, with a reference value of γ=1.33 similar to the approach suggested in [35] (i.e. removing combinations of high unburnt temperature with low pressure and vice-versa, where the adiabatic compression ideal profile is strongly modified).

The fitted correlation is based on a modified version of that reported by Cazzoli et al. [21], and it is represented by the set of equations:

$$\begin{cases} s_l = s_{l_0} \cdot f_1(T,\phi) \cdot f_2(P,\phi) \cdot f_3(X_{EGR},\phi) \cdot f_4(X_{H_2O},\phi) \\ s_{l_0} = 14.78 \cdot e^{-\frac{(\phi-1.1)^2}{0.1285}} + 5.69 \cdot \phi - 1.58 \cdot \phi^2 \\ f_1(T,\phi) = (T/400)^{2.43+0.125\cdot(\phi-1.1)} \\ f_2(P,\phi) = (P/50e5)^{0.236+0.226\cdot(\phi-1.1)} \\ f_3(X_{EGR},\phi) = 1 - 1.79 \cdot (X_{EGR})^{0.726+0.162\cdot(\phi-1.1)} \\ f_4(X_{H_2O},\phi) = 1 - 2.47 \cdot \left(X_{H_2O}\right)^{0.755+0.328\cdot(\phi-1.1)} \end{cases} \qquad (7)$$

As can be seen from Figure 4 the effect of water addition in reducing the laminar flame speed is a function not only of the water mass fraction, but also of the equivalence ratio of the mixture, while it results almost independent from the temperature level. In order to keep into account this dependence, the term f_4 is not a linear relationship with X_{H_2O}, but depends also on the equivalence ratio.

The results obtained with the correlation are reported in Figure 5 in terms of laminar flame speed for 2 operating conditions and different values of X_{H_2O}, identified as LP (T_u= 600 K, P = 30 bar) and HP (T_u= 900 K, P = 140 bar). It should be noticed that the results show a regular profile without spurious oscillations also for values of the equivalence ratio far from stoichiometric, which is a problem seldom found in this kind of correlations [22].

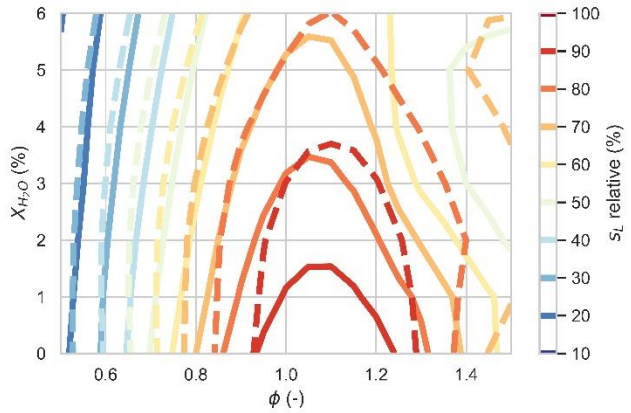

Figure 4. Relative LFS as a function of equivalence ratio and water mass fraction for P=60 bar and T=600 K -, T=900 K - -

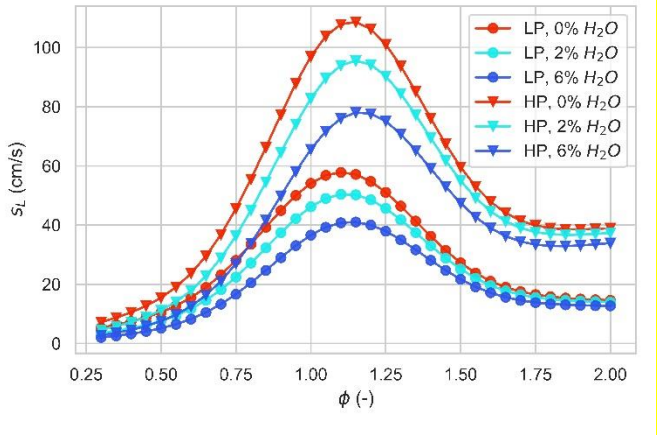

Figure 5. LFS correlation results as a function of equivalence ratio and water mass fraction for different operating conditions

Methodology focused on ignition delay derivation

In order to reflect the conditions observed during a reflected shock tube experiment, a 0D model of a constant volume adiabatic reactor has been applied to define the ignition delay time of a surrogate mixture under defined initial conditions. Considering the size of the domain, the time required to run a detailed chemistry simulation is considerably smaller than that needed for laminar flame speed calculations (in the order of 10 s for condition with the POLIMI scheme), therefore there is no need to reduce the mechanism for this application. The adopted gasoline fuel surrogate is consistent with the choice for the laminar flame speed. Experimental data are not available for this surrogate, therefore the POLIMI mechanism has been validated for ignition delay time simulations against a different surrogate composed by the same components (surr_A composition: 16.9% (vol.) n-heptane NC7H16, 62.9% iso-octane IC8H18, 20.2%(vol.) toluene C7H8) available in literature [36]. The results for different equivalence ratios normalized at a pressure of 52 bar are reported in Figure 6. The simulations show a good agreement for temperatures higher than 900 K, while tend to underestimate the ignition delay time at lower temperatures, especially for the rich mixture.

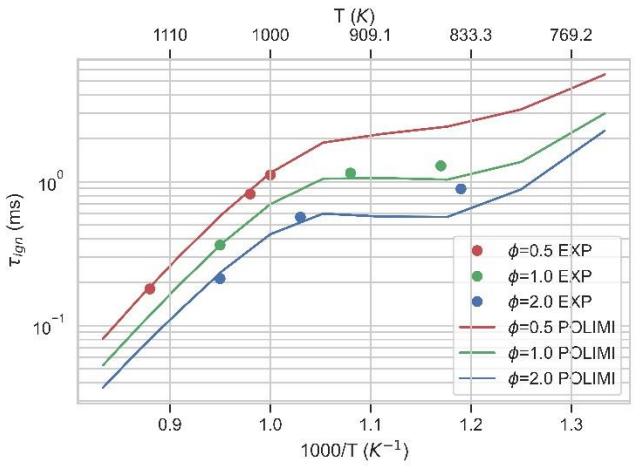

Figure 6. Ignition delay time of surr_A for different equivalence ratios and temperatures at P=50 bar

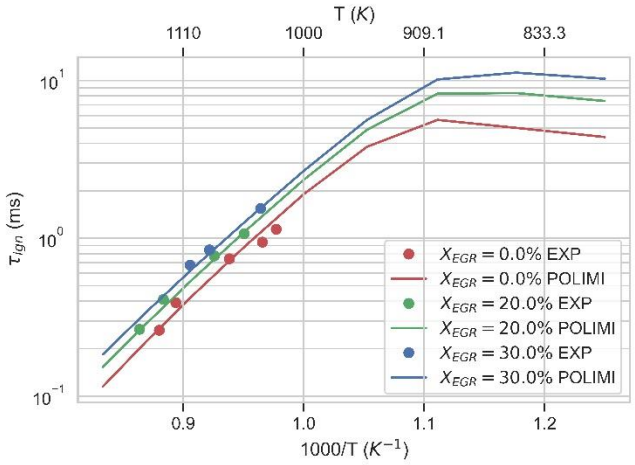

Figure 7. Ignition delay time of surr_A for different EGR mass fractions and temperatures at P=20 bar

The effect of water vapor addition to the reacting mixture has never been registered experimentally, to the best knowledge of the authors, and therefore the validation results of the sensitivity of the detailed chemical kinetics simulations with respect to a diluent addition have been performed with respect only to EGR. The results reported in Figure 7 compare the experimental [36] and calculated values of ignition delay time for the surr_A at P=20 bar, ϕ=1.0 and different fractions of EGR (0%, 20%, 30%). The comparison between experimental data and the results of the simulations show a good agreement both in terms of absolute value and sensitivity to diluent addition.

The simulations have been performed for a wider grid than the one needed for LFS definition, reported in Table 5, since knocking phenomena can generate higher levels of temperature and pressure that must be accounted for. The size of the dataset, however, is similar to the previous one, since the sensitivity of the ignition delay time to the equivalence ratio is lower and allows the adoption of fewer breakpoints along its axis (Table 7).

Table 7. Grid points for ignition delay time simulations

	Min/max	# points
P (bar)	5 – 200	10
T_u (K)	650 – 1400	20
ϕ (-)	0.3 – 2.5	8
X_{EGR} (%)	0 – 30	5
X_{H_2O} (%)	0 – 6	4

The definition of the correlation is based on the work of [36] but includes the effect of the addition of diluents to the reacting mixture, represented by a linear correlation. The effect of pressure, temperature and equivalence ratio are represented by three terms (R1, R2 and R3), initially specified for different temperature levels. The coefficients for the correlation have been optimized by minimizing a custom error function defined as:

$$J = 0.7 \cdot |\tau^* - \tau|_1 + 0.2 \cdot |\tau^* - \tau|_2 + 0.1 \cdot \max(|\tau^* - \tau|_1) \quad (8)$$

τ^* represents the ignition delay time predicted by the correlation and τ is the value obtained with the detailed chemistry simulation. Subscript 1 indicates the area of the grid that the engine is more likely to reach during operation, while 2 represents the remaining points. Differently from the LFS application, region 1 is limited only by the equivalence ratio ($0.5< \phi <1.5$) since, in case of knocking events, the relationship between P and $T_u$would be difficult to predict. The fitted correlation is reported in the following system:

$$\begin{cases} \tau_{IGN} = \frac{1e3}{(R1+R2)^{-1}+R3^{-1}} \cdot R_{dil} \\ R1 = 3.1e-17 \cdot P^{0.05} \cdot e^{\frac{1.78e4}{T}} \cdot \phi^{-0.3} \\ R2 = 5.42e2 \cdot P^{-1.37} \cdot e^{\frac{2.12e3}{T}} \cdot \phi^{-1.3} \\ R3 = 8.75e-7 \cdot P^{-0.97} \cdot e^{\frac{1.52e4}{T}} \cdot \phi^{-0.36} \\ R_{dil} = (1 + 1.745 \cdot X_{EGR}) \cdot (1 + 1.38 \cdot X_{H_2O}) \end{cases} \quad (9)$$

The results of the correlation are reported in Figure 8 as a function of temperature and water mass fraction for two engine relevant conditions identified as LP (ϕ=1.0, P=30 bar) and HP (ϕ=1.0, P=140 bar). The correlation displays a different sensitivity to the NTC (Negative Temperature Coefficient area, where the temperature level is more likely to be reached by the reacting mixture) behavior with increasing pressure, in agreement with the results of the detailed chemical simulations and experimental data. The effect of water addition results, however, less effective than the addition of EGR in reducing the reactivity of the mixture and, thus, increasing the ignition delay time.

The correlations previously found for the LFS ant IDT evaluation have been used for the engine three-dimensional CFD simulations presented in the forthcoming sections. The implementation of the LFS and IDT correlations and the coupling with the main combustion model in the FIRE CFD code has been done by means of user-coding.

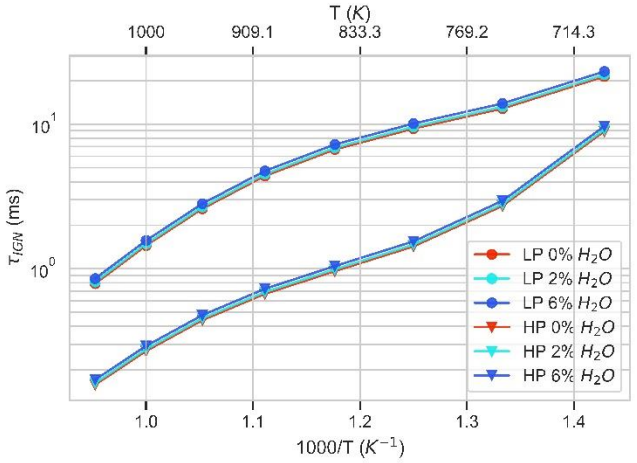

Figure 8. Ignition delay time obtained with the correlation for different temperatures and water mass fractions in 2 different operating conditions

WATER INJECTION SYSTEM AND ENGINE CONFIGURATIONS: NON-REACTING FLOW RESULTS

The current turbocharged SI engines fuel enrichment strategy (component protection strategy) adopt a mixture index variable in the range among λ 0.75 and λ 0.85 for limiting TiT under the threshold value (i.e., 950 °C) imposed by current turbine material thermal limits. For environmental protection pursuit, soon the gasoline engines will likely need to run under stoichiometric conditions. In order to highlight the consequences of such a shift from rich mixture to stoichiometric mixture operations, the performances of the analyzed engine at full power operating point (which is indeed the most demanding one) have been set at λ 0.75, λ 0.85 and λ 1.0. These results represent a mandatory comparison for the assessment of the simulation results obtained by applying the water injection strategy under stoichiometric conditions. Then, a selection of the best cases for both PWI and DWI configurations under not-reacting flow conditions will be presented and discussed. The water injection cases have been run at full power condition, at the same rated power engine speed by varying: i) *the injection pressure*; ii) the *injection timing*; iii) *the parameter s (i.e., the non-dimensional water injected)*; iv) *the compression ratio CR*. A final summary comparison between PWI and DWI system performances under reacting flow conditions will be presented at the end of the research paper. In Table 8 the analyzed cases for both PWI and DWI systems have been reported. The injection pressure for DWI strategy has been chosen in the range between 50 bar and 150 bar, i.e. respectively the lowest and maybe the highest-pressure level for the DWI solution. The lowest injection pressure (i.e. 50 bar) may be the most feasible forecast solution in a near term because of the injection system costs. The PWI injector spray pattern was oriented toward the intake valve in order to target properly the cylinder minimizing the impact of liquid water against intake and port walls as well as intake valve stems and seats. The injection timing was set to allow the spray entering the cylinder. Thanks to the latter, the water spray takes the advantage of the more favorable thermodynamic conditions for the evaporation process than those it could face in the intake manifold and ports. The relative injection pressure was set to 10 bar for using the current PFI and UREA technologies, thus reducing costs. An injection pressure lower than 10 bar reduces the flexibility in the injection timing selection and sweep, as already discussed by the authors in [2]. Injection

pressures greater than 20 bar are beyond the practical interest because of the associated costs.

Table 8. PWI and DWI – Analyzed cases

WATER INJECTION SYSTEM	Parameter s [-]	Injection pressure [bar]
DWI	0.25 / 0.35 / 0.55	50.00 / 150.00
PWI	0.20 / 0.30 / 0.40	10.00

Table 9. PWI, DWI and engine configurations - Operating points for reacting-flow analyses – Fixed Power and Bmep target

H2O INJ. SYST.	Parameter s [-]	Inj. Press [bar]	CR
DWI	0.35	50.00	9.5
		150.0	9.5
			10.5
	0.55		9.5
PWI	0.30	10.00	9.5
			10.5

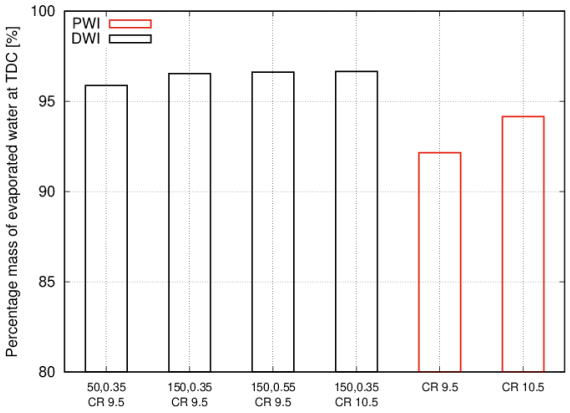

Figure 9. Percentage of evaporated water mass at TDC – NON-REACTING FLOW

For drawing the best solution between the analyzed cases, it was necessary to define the following selection criteria:

1. The 90% of the injected water mass must evaporate.
2. Cooling temperature versus the reference case λ 0.75.
3. Cooling efficiency: it assesses the quantity of wasted water, i.e. useless for mixture cooling purposes.

In Table 9 the best cases accomplishing the above three constraints have been reported and they have been adopted for further combustion analysis. Moreover, for these cases the engine configuration was varied in terms of Compression Ratio CR, too. A value of CR higher than 10.5 was not feasible because of the intrinsic drawing limits in the present combustion system baseline geometry. In Figure 9 the percentage mass of the evaporated water for both the PWI and DWI solutions is depicted at TDC. It is to highlight that the imposed constraint of at least 90% of evaporated mass has been respected in all cases. This is an important feature that should be fulfilled, at least by means a CFD simulation check, in the water injection system assessment in order to not waste water.

To evaluate the performance of the water injection strategy it is necessary to consider both the cooling of the mixture temperature at IVC/TDC and the effective quantity of injected water mass useful in this cooling process (cooling efficiency). These two parameters have been analyzed in detail for cases of Table 9 only, because they are of interest for the reacting flow analysis.

Water Cooling Effect on the Non-Reacting Mixture

In Figure 10 the temperature difference using as REFERENCE the FUEL-ONLY CASE at stoichiometric condition (i.e., λ 1.0) at TDC is shown. Mass-averaged in-cylinder temperature lower values indicate a better charge cooling while higher values denote possible knocking issues and NOx emission increase, as well as the risk to overcome the TiT threshold. Moving from λ 0.75 (i.e. L 0.75 in the figure) to λ 0.85 (i.e. L 0.85 in the figure), there is a decay of the temperature difference, due to both the reduction of the injected fuel (the less the injected fuel, the less the heat subtracted to the mixture during the evaporation process) and the increase of the heat capacity ratio of the mixture (mixture chemical variation). The DWI water injection results in a remarkable temperature difference versus the reference case λ 0.75, as shown in Figure 10. The greatest cooling effect is achieved for the case 150 bar, s 0.55.

For PWI strategy, the lowest temperature (i.e., the highest temperature difference with respect to the reference case) at TDC is reached for case CR 9.5. The CR increase penalizes the final temperature level at TDC. For the same engine geometry (CR 9.5) the best DWI solution, represented by injection pressure 150 bar and parameter s 0.55, more than doubles the cooling effect of the corresponding PWI solution. Then, from above appears the greater potential of DWI system than PWI architecture in terms of water consumption despite the expected larger cost of the solution (high-pressure injector, high-pressure pump with technology challenge in reliability) and other concerns like those relying the water injector reliability and lubricant contamination.

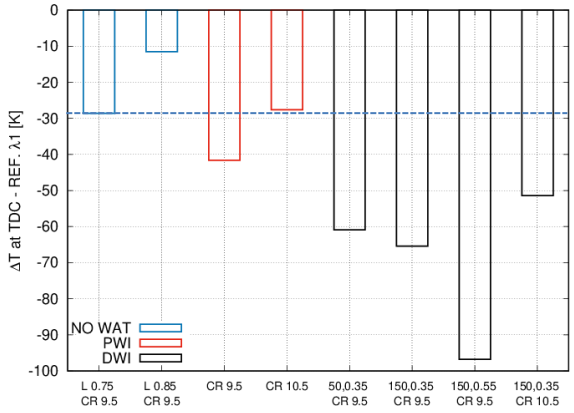

Figure 10. Temperature difference for FUEL-ONLY NON-REACTING FLOW - Mixture index moved from 0.75 to 1.00, w/ and w/o injected water – REFERENCE CASE λ 1.0 at TDC

The temperature evaluation, compared to the stoichiometric case without water injection (REFERENCE CASE), is then a measure of the net performance of the water injection. The temperature difference with respect to the reference case increases with the injected water mass but not linearly. Part of the injected water remains liquid or vaporizes but not from the spray or the wallfilm on the walls, so it is useless in the thermodynamic balance of the mixture cooling.

The cooling efficiency $\eta_{COOLING}$ was introduced by the authors in the present paper to assesses the *quantity of wasted water*, i.e. injected but useless for the mixture cooling. The cooling efficiency $\eta_{COOLING}$ was defined as the ratio between the effective temperature decrease reached at TDC (ΔT_{REAL}) and the ideal (maximum) temperature decrease (ΔT_{IDEAL}) reachable under the hypothesis of instantaneous (isochoric) vaporization of 100% of the injected mass of water at SOI conditions, both at the stoichiometric condition:

$$\eta_{COOLING} = \frac{\Delta T_{REAL}}{\Delta T_{IDEAL}} \qquad (10)$$

$$\Delta T_{IDEAL} \cdot c_V \cdot m_{CYL} = m_{H2O} \cdot LHV_{H2O} \qquad (11)$$

Where m_{CYL} and m_{H2O} are respectively in-cylinder mixture and injected water mass, LHV_{H2O} is the water latent heat of vaporization and c_V is the specific heat at constant volume of the mixture.

It was chosen to consider the boundary conditions at SOI for 'weighting' the thermodynamic gap between PWI (intake) and DWI (in cylinder) boundary conditions of pressure and temperature [1, 2].

In Figure 11 the cooling efficiency is depicted depending on the injection pressure: 50 bar and 150 bar for DWI strategy, 10 bar for PWI strategy. For PWI, there is a systematic decrease of the efficiency increasing the injected water mass. This is due the local saturation limit, which is even closer increasing the water mass quantity (increase of parameter s). The DWI case s 0.55 has the lowest efficiency and the higher mixture cooling (Figure 10). The efficiency of the PWI strategy is always lower than the efficiency of the DWI strategy, as one can expect.

In Table 10 the injection phasing, which is independent by the engine configuration (CR), for both fuel and water has been summarized.

In Figure 12 the mean in-cylinder turbulent intensity has been reported for both DWI and PWI solutions. It is to highlight that there is a penalization of the mean in-cylinder turbulent intensity for DWI strategy, while there is an increment in case of PWI strategy, if compared with the fuel-only case. These results depend on the SOI timing during the suction phase and so on the spray jet momentum, which interacts with the main in-cylinder flow. The highest level of turbulent intensity is at CR 9.5 for the DWI s 0.35-150 bar case, and at CR 10.5 for the PWI solution.

WATER INJECTION SYSTEM AND ENGINE CONFIGURATIONS: REACTING FLOW RESULTS

In modern turbo-charged engines working under stoichiometric conditions it is not enough to verify that, for a given load, the chosen spark advance is KNOCK SAFE, but it is necessary that the average exhaust gas temperature at turbine inlet (namely TiT) remains below 950°C particularly in the map region close to the rated power.

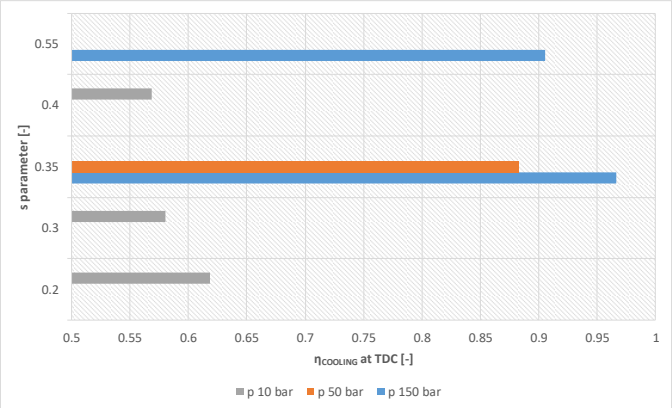

Figure 11. Cooling efficiency at TDC for: i) DWI (injection pressures 50 and 150 bar); ii) PWI (injection pressure 10 bar) – NON-REACTING flow – CR 9.5

Table 10. Gasoline, Port Water and Direct Water injectors: injection timing

TYPE OF INJECTOR	Injection pressure [bar]	Parameter s [-]	SOI [CA deg. ATDCF]	EOI [CA deg. ATDCF]
GASOLINE	350.0	-	378	532
DWI	150.0	0.35	418	506
DWI	150.0	0.55	396	527
DWI	50.0	0.35	390	533
PWI	10.0	0.30	293	433

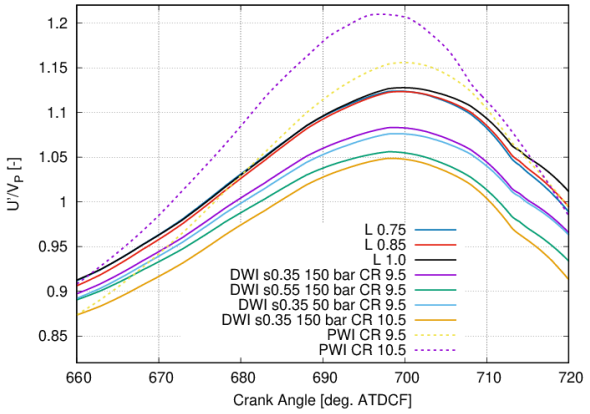

Figure 12. Mean in-cylinder turbulent intensity u'/VP - NON-REACTING FLOW

Then, the engine map must be verified for the fulfillment of both engine knock-safe operations and exhaust gases TiT limit. As far as the latter is concerned, it must be considered that upcoming turbocharger technologies are increasing the TiT limits up to 1030-1050°C. Since the present work deals with 3D CFD in-cylinder simulations, the exhaust gas threshold temperature value representative of the TiT limit was taken as 1630 °C (that corresponds to 1903.15 K) at 800 CA deg. ATDCF, based on an estimation carried out in OpenWAM 1D simulations.

In the present work, the incipient knock condition was identified by using as threshold MAPO limit the BOSCH criterion, which is obtained dividing the engine speed (in rpm) by 1000. A 4th order Butterworth band-pass filter between 5kHz and 20kHz for evaluating the MAPO has been applied to the pressure trace in a crank angle window between -10 and 80 crank angle degrees after top the dead center (ATDC) [38]. The pressure trace was recorded by a virtual probe flush mounted on the cylinder head close to the location of the water injector (the probe location is the same for both configurations). To define a practical rule for determining the Knock Limit Spark Advance KLSA, the latter is the SA undergoing the condition of incipient detonation minus 4 crank angle degrees in order to include the cycle to cycle variation stochastic effect.

Finally, it is to say that the combustion angles have been derived by the virtual transducer pressure trace using post-processing analysis methods as those used at the test bench for the indicating data analysis.

A brief overview on the combustion simulation WITHOUT water injection

The actual fuel enrichment strategy for limiting TiT below the threshold adopts a mixture index variable in the range among λ 0.75 and λ 0.85. The reference case for the present combustion strategy has been chosen to be λ 0.75: case λ 0.85 is a less favorable point for the combustion development, due to its higher temperature at TDC, as in Figure 13b. The stoichiometric condition (λ 1.0) has been compared to both cases. Main results will be traced on the MFB50 (50% mass fraction burnt) parameter, which represents the combustion phasing of the engine [21].

The methodology here proposed, based on the detailed evaluation of the chemical properties of the mixture (and not only of the fuel), and therefore of its reactivity, allows properly simulating the evolution of the flame under variable quantities of water vapor, and not only as a function of pressure, temperature, mixture index, as well as EGR, whose chemical properties are different from those of the injected water, as already demonstrated [3, 4].

For the combustion analysis, in Figure 13 the trend of the MAPO value versus both the MFB50 and the mean exhaust temperature has been reported. In Figure 13b, where the MAPO versus the exhaust temperature is visible, only the SA laying in the bottom left of the graph, i.e. below the MAPO THRESHOLD and to the left of the EXHAUST TEMPERATURE THRESHOLD are truly workable. This area represents the 'acceptability zone': each SA falling outside this zone is not acceptable or for possible knock onset or for temperature greater than the TiT or both. Depending on the mean mixture index, SA inducing the engine to work with MFB50 lower than 15-18 CA deg. are subject to detonation. The only feasible operating condition is λ 0.75 because in the only laying in the 'acceptability zone', thus, at full power condition, the engine works only at λ 0.75. Both the λ 1.0 and the λ 0.85 cases, at the knock safe advance points (below the YELLOW LINE of maximum MAPO), do not respect the maximum temperature constraint.

In Figure 14 the normalized IMEPH versus the MFB50 parameter is visible: the IMEPH value was computed in the range 690 – 800 CA deg. ATDCF. The reference IMEPH-TARGET value is that of the knock safe SA at λ 0.75 and it corresponds to the engine BMEP target. It must be noted that authors refer to IMEPH target rather than BMEP target to perform the comparison within the three-dimensional CFD simulation framework of analysis.

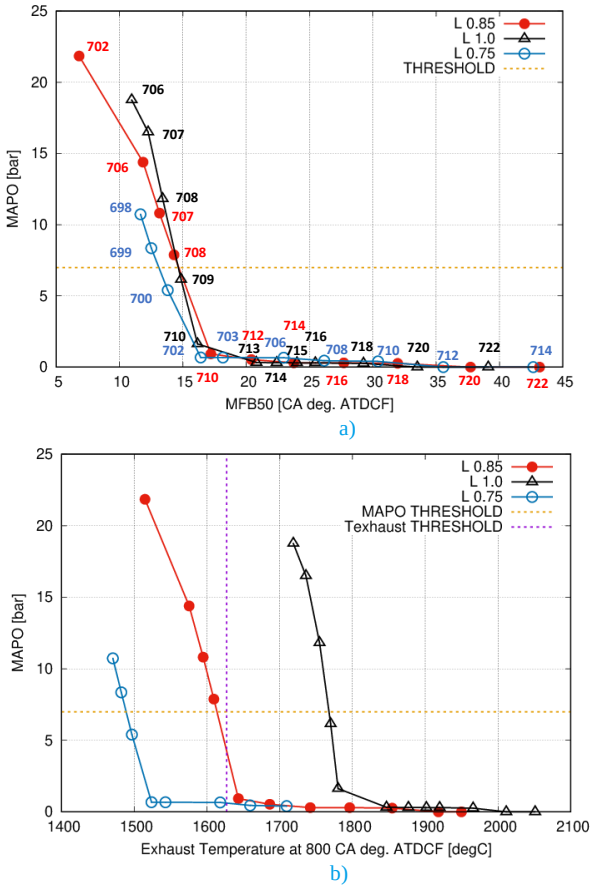

Figure 13. Maximum Amplitude of Pressure Oscillations versus: (a) MFB50; (b) Exhaust temperature at 800 CA deg. ATDC

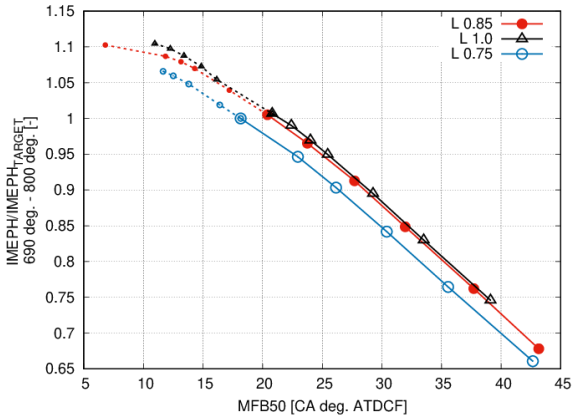

Figure 14. - IMEPH/IMEP$_{TARGET}$ swept versus MFB50 – KNOCKING SA in DASHED LINE

The IMEPH value plotted in the picture was normalized by the IMEPH target value. A value of this ratio greater than 1.0 means an excessive load if compared to the target. In Figure 14 the knocking SA are in dashed lines: the knock safe SA for each considered mixture index are those at the boundary between dashed line and continuous line. It is to note at fixed target IMEPH value that the KLSA at λ 0.75 is 703 CA deg. ATDCF, the KLSA at λ 0.85 is 712 CA deg. ATDCF and the KLSA at λ 1.00 is 713 CA deg. ATDCF. The in-cylinder thermal regime is higher for λ 0.85 and λ 1.00 than for λ 0.75 (Figure 10). Case λ 0.85 reaches the same IMEPH of λ 1.00 but with a SA less of 1 degree than λ 1.00: for understanding this, it is necessary to consider the laminar flame speed in Figure 15.

The laminar flame speeds of cases λ 1.00 and λ 0.85 are quite the same except for the combustion initial phase (which is indeed the most important phase of premixed combustions), where the case λ 1.00 shows the faster values because of the mixture inhomogeneity close to the spark plug at ignition time. The case λ 0.75 presents a much lower laminar flame speed, as visible in Figure 15 because of the adopted air index. Thus, to achieve the target IMEPH the spark angle must be advanced of about 10 degrees, in order to compensate the slower flame laminar speed. This operation is made feasible without knock limitation due to the lowest thermal regime, as shown in Figure 10, where one can see that the case λ 0.75 provides the lowest unburnt gas temperature.

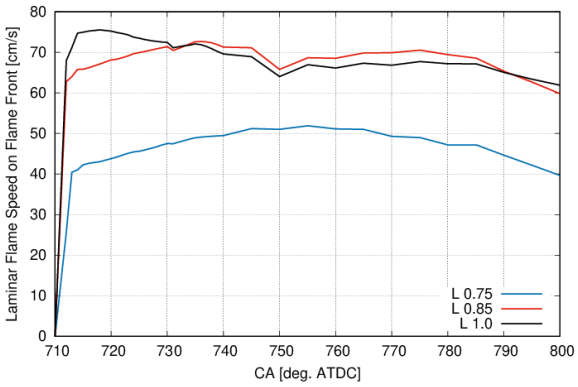

Figure 15. Laminar flame speed on flame front at SA710 CA deg. ATDCF.

For summarizing, the previous results show the limitation occurred in operating the engine at λ 0.85 and at λ 1.00 due to the higher thermal in-cylinder conditions than that occurring in the case at λ 0.75. The challenging is the fulfillment of the exhaust gas TiT limits. The temperature at 800 CA deg. ATDCF of the present engine should be lower than 1630 °C (1903,15 K), representative of the TiT limit for the turbine protection issues. Only the case at λ 0.75 fulfills the TiT limit. For both cases at λ 0.85 and at λ 1.00, this constraint is not satisfied since the TiT cannot be lowered by increasing the spark advance because of the knock onset.

As a result, the stoichiometric case at full power, which may be likely required by new AES assessment policy, is expected to not largely fulfil current turbocharging TiT limits. Thus, the challenge of dealing with TiT limit at stoichiometric condition is assessed in the next paragraph with the application of the water injection.

Combustion simulation WITH water injection

Applying the water injection strategy, the fresh gases temperature has been reduced as a function of the injected water mass as shown in the Figure 10. Therefore, one can start drawing some considerations about the key points of the forthcoming combustion analysis:

1. The main result expected by using the water injection is to have a wider choice in setting the best Spark Advance (SA) because the knock risk is kept far away;
2. On the other hand, it is necessary to keep in mind that the water acts as inert gas penalizing the laminar flame speed of the burning mixture. Moreover, the lower fresh mixture temperature slows down the laminar flame speed. Then, there is an ‘a priori penalization’ of the combustion in the water injection concept itself, with a risk to not achieve gain on TiT reduction. In this contest, approaches based on complex chemistry are mandatory to perform accurate assessments of the water injection system technology and operations which face the compromise between the enhancement of an efficient mixture cooling effect and the reduction of the exhaust gas temperature.

The best configurations tested for PWI and DWI solutions have been summarized in Table 9: they will be analyzed in detail considering in first step the cases with the same engine compression ratio (i.e., CR=9.5).

It is possible to compare simulation results following two approaches:

1. Same IMEPH to the target value obtained for case λ 0.75: in this case the ratio IMEPH on $IMEPH_{TARGET}$ is 1.00 or close to it. In this case it is highlighted how the same load can be reached with a reduced spark advance, thanks to reduced pumping losses, better surface-to-volume ratio S/V being the combustion shifted toward TDC, where S/V is optimal.
2. IMEPH evaluated at knock limited SA: in this case it will be shown that the ratio IMEPH on $IMEPH_{TARGET}$ is greater than 1.00, which means that the load might be reduced up to the target one, i.e. the quantity of fuel has to be lowered (fuel consumption and boost pressure reduction for fixed mixture index), which allows reducing the thermal load too. In this case the maximum load obtainable by the new configuration is highlighted.

Engine type: CR 9.5 – PWI vs DWI

In Figures 16 and 17 are shown respectively the normalized IMEPH curves versus MFB50, the MAPO curves versus MFB50 and exhaust temperature at 800 CA deg. ATDCF. It is clearly visible that the DWI strategy never shows knock onset at the injection pressure of 150 bar because the MAPO curves never approach the threshold line of 7 bar, while it detonates at 50 bar for SA 694 (Figure 17). At this spark angle, the MFB50 angle is 6.0 CA deg. ATDCF: water has increased the tolerability threshold of the engine to a faster cycle than the average one typical of this type of engine. In Figure 17b it is to note that the case s 0.35 50 bar cannot reach the ‘acceptability area’ of the engine, i.e. it is not possible to lower the temperature below the threshold temperature and, at the same time, to keep the MAPO in the safe zone. Looking at Figure 16, the DWI solution allows to increment the SA obtaining high IMEPH values, above the target one: the advance allows speeding up the combustion and it reduces the exhaust temperature. Therefore, a high IMEPH is obtained with the same FUEL CONSUMPTION, that means a reduction of the *bfsc*. In general, it can be stated that DWI systems result in lower in-cylinder thermal load than PWI with a gain *on the bfsc*. Nevertheless, it must be pointed out that the in-cylinder exhaust gas temperature at 800 ca deg. ATDCF does not fall below the threshold because of the slowdown of the flame speed. The last is linked both to the presence of significant mass fractions of water in the vapor state and to the drop of the mixture temperature. The laminar flame speed is mainly influenced by these last two parameters, mostly the quantity of vaporized water.

In Figure 18 the combustion durations MFB10-MFB50 and MFB50-MFB90 are shown. The low pressure DWI case (s 035 p 50 bar) has a slow combustion phase as the high pressure DWI (150 bar) strategy but does not have its 'thermal advantage' for the fresh mixture (Figure 19), so it reaches the knocking onset in the end-zone of the chamber.

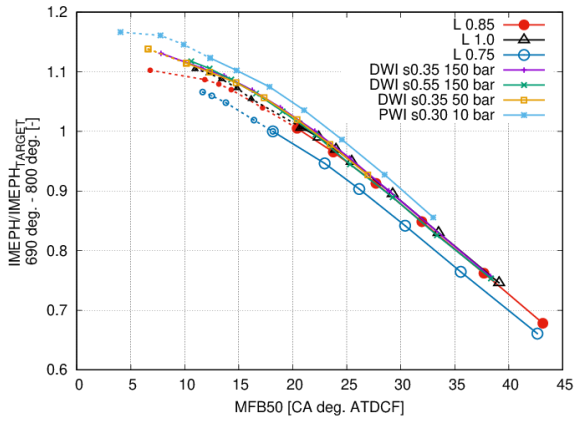

Figure 16. - IMEPH/IMEPTARGET swept vs MFB50 – KNOCKING SA in DASHED LINE

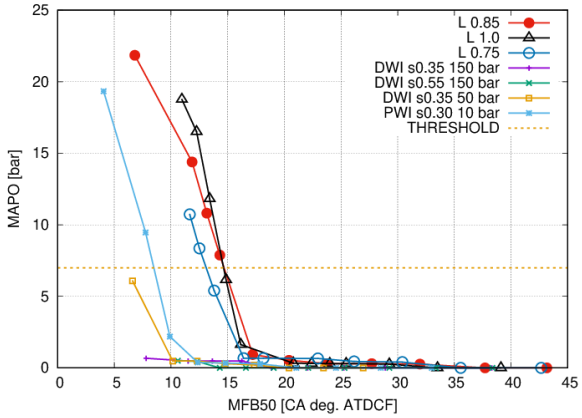

(a)

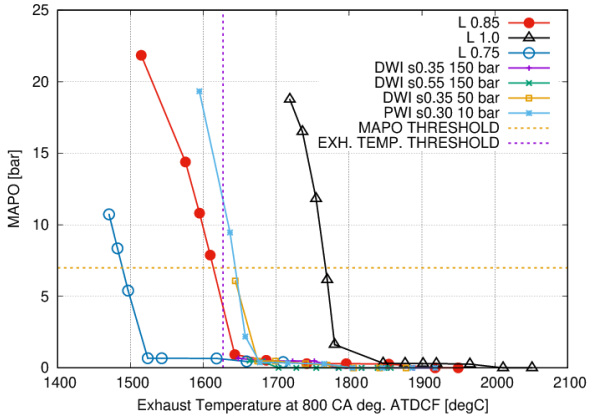

(b)

Figure 17. Maximum Amplitude of Pressure Oscillations versus: (a) MFB50; (b) Exhaust temperature at 800 CA deg. ATDC

In Figure 18 for both combustion durations it is very clear that the case with s 0.55 has too slow combustion phase: it does not reach the 99% of MFB even at SA 702 CA deg. ATDC because it has a lot of evaporated water and together also very low temperatures. The whole result is a slowdown of the combustion process. So, the case s 0.55 is interesting if only the fresh mixture temperatures are considered, but it is not practically feasible for its combustion deceleration.

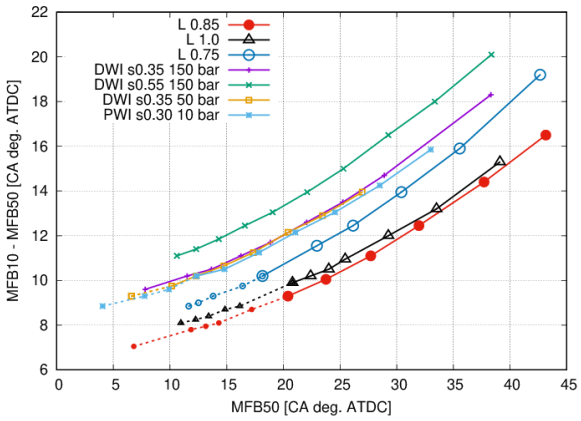

(a)

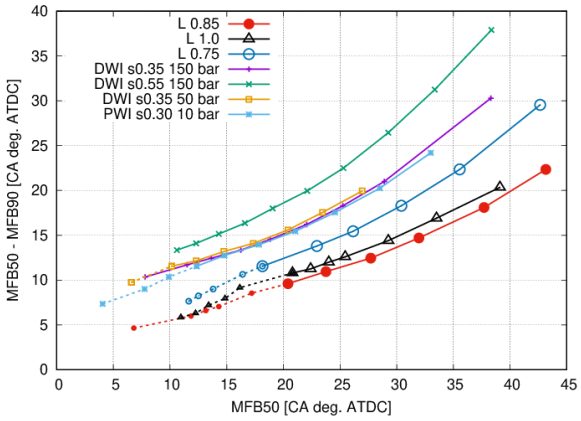

(b)

Figure 18. – Combustion duration vs MFB50: (a) MFB10 to MFB50; (b) MFB50 to MFB90

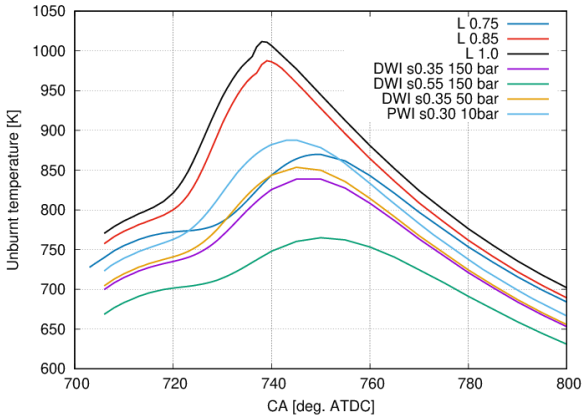

Figure 19. Mean temperature of the unburnt mixture at SA706 CA deg. ATDCF.

Summarizing what has been stated so far:

1. The laminar flame speed is MAINLY INFLUENCED by the reactivity of the mixture, therefore by the chemical properties the mixture assumes depending on the quantity of vaporized water, which lowers the temperature but also acts as an inert. Accurate modeling of the chemistry is thus mandatory.
2. The case s 0.55 leads to a very low in-cylinder thermal level but at the expense of an excessive combustion slowdown, therefore it is not of interest for engine applications.

The above presented results for DWI strategy show that the achievable load is greater than expected (BMEP TARGET 26.6 bar), so it is certainly possible to reduce the quantity of fuel, which in itself already reduces the engine exhaust temperature and in general the thermal load of the engine cycle. The cooling margin in comparison with the rich mixture solution (λ 0.75) allows investigating solutions with increased CR, which is limited in the present work to CR 10.5 for engine geometry reasons.

Engine type: CR 10.5 – PWI vs DWI

In this paragraph cases at CR 10.5, respectively DWI s 0.35 - 150 bar and PWI s 0.30 - 10 bar, are analyzed. In Figures 20 and 21 are shown respectively the normalized IMEPH curve versus MFB50, the MAPO curves versus MFB50 and exhaust temperature at 800 CA deg. ATDCF. In Figure 22 the laminar flame speed on flame front is depicted for both DWI and DWI solutions. By them it is possible to compare DWI and PWI systems for the same engine type:

1. For the same target IMEPH value, the DWI system gains 1 deg. in the SA at the same exhaust temperature.
2. Looking at the knock safe SA, so considering the maximum performances of the engine, the DWI system gains 6 CA deg. in the knock safe SA, resulting in a 1% increment of the IMEPH value and the exhaust temperature reduces of almost 100.0 K.
3. The CR increase induces a higher laminar flam speed (Figure 22). The laminar flame speed is higher for PWI strategy than for DWI strategy because of both the higher thermal regime associated to the PWI solution and the less water vapor mass (s 0.30 instead of s 0.35).

It is also possible to compare the effect of the increased CR for the same water injection system:

DWI: Increasing the CR of 1.0 in the DWI system, the knock safe SA is shifted towards TDC of 2 degrees, while the IMEPH is almost the same. The exhaust temperature is reduced of 40.0 K. At SA 700 CA deg. ATDCF, which is the knock safe SA for DWI CR 10.5, there is an exhaust temperature reduction of 77.0 K if compared to the same system having CR 9.5. The last is due to the more efficient combustion process linked to the increased thermodynamic efficiency, which reduces the combustion angles. In general, increasing the compression ratio of 1.0, there is an increment of the IMEPH (Figure 20). The IMEPH value, at the same SA, increases of about 2%: it is possible to reduce the fuel consumption, as just observed before. Increasing the injected water, at the same SA the IMEPH gets reduced because of the slowdown of the combustion (MFB50 lengthening). The DWI solution at increased CR reaches the knock onset because the combustion duration is a little higher (Figure 23) but the mixture temperature is higher too.

PWI: Increasing the CR of 1.0 in the PWI system, the knock safe SA is anticipated of 4 degrees, i.e. it is 706.0 CA deg. ATDCF instead of 702.0 CA deg. ATDCF: the exhaust temperature increases from 1950.0 K to 2007.0 K. The normalized IMEPH reduces from 1.12 at CR 9.5 to 1.09 at CR 10.5. The SA at target IMEPH is shifted towards TDC of 1 degree, with an exhaust temperature reduction from 2119.0 K to 2080.0 K at CR 10.5.

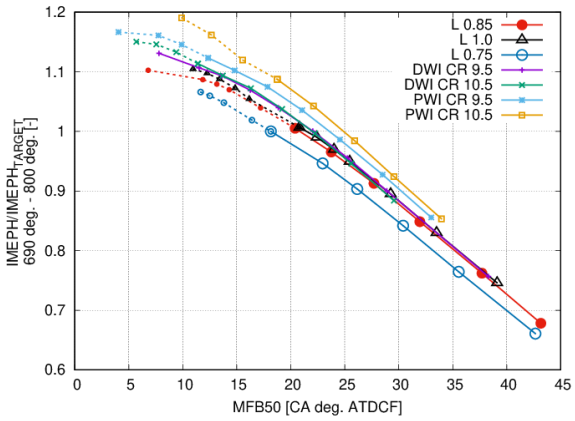

Figure 20. - IMEPH/IMEPTARGET swept vs MFB50 – KNOCKING SA in DASHED LINE – DWI: s 0.35 150 bar – PWI: s 0.30 10 bar

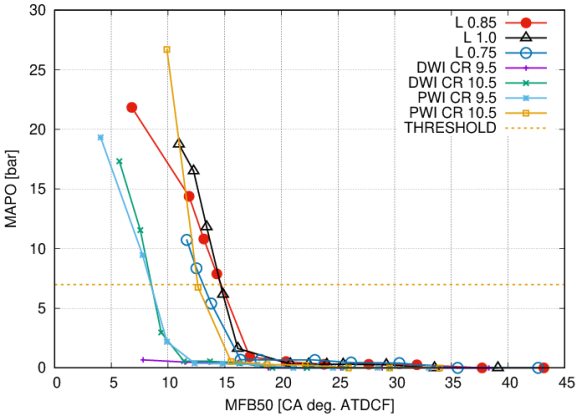

(a)

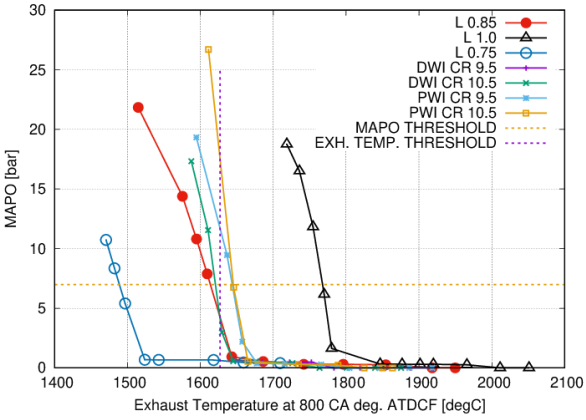

(b)

Figure 21. Maximum Amplitude of Pressure Oscillations versus: (a) MFB50; (b) Exhaust temperature at 800 CA deg. ATDC – DWI: s 0.35 150 bar – PWI: s 0.30 10 bar

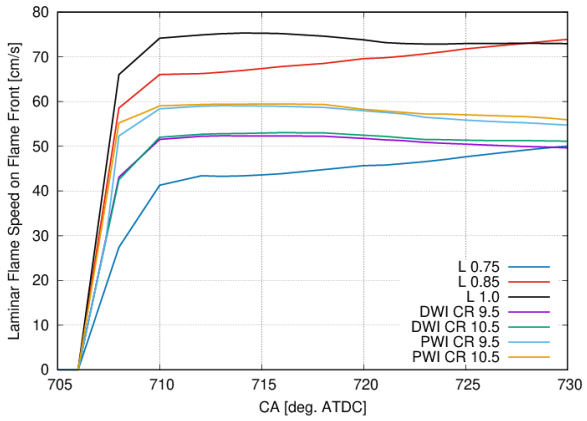

Figure 22. Laminar flame speed on flame front at SA706 CA deg. ATDCF.

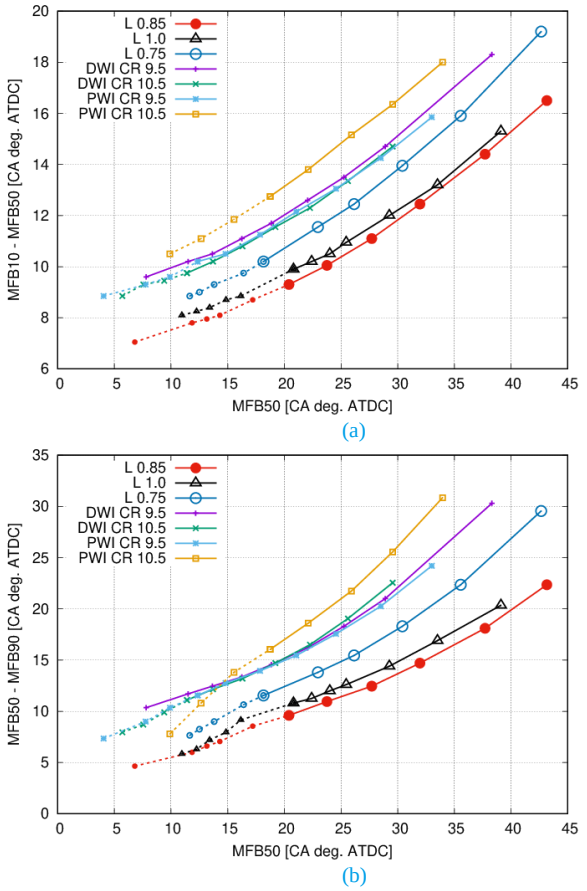

Figure 23. – Combustion duration vs MFB50: (a) MFB10 to MFB50; (b) MFB50 to MFB90 – DWI: s 0.35 150 bar – PWI: s 0.30 10 bar

Summarizing, in PWI system the CR increase induces an anticipation of the knock safe SA with a loose of 60.0 K in the exhaust temperature, and the IMEPH target is reached at SA 709.0 CA deg. ATDCF instead of 710.0 CA deg. ATDCF, with a reduction in the exhaust temperature of 40.0 K. Globally there is a lengthening of the combustion duration increasing the CR in PWI systems (Figure 23).

The increase in CR decreases the cooling effect of the water in compression (at the same IMEPH, it is not worth mentioning) but it is found to: a) increase the thermodynamic efficiency thanks to a larger expansion phase and to higher laminar flame speeds (Figure 22) which shortens the combustion durations; b) reduce the exhaust gas TiT value, as overall results of the previous point.

Conclusions

In the present work, a complete methodology for the simulation of internal combustion engines under water injection conditions has been described. New correlations for the laminar flame speed, thickness and ignition delay time have been developed and fitted against a complete dataset of detailed chemical kinetics simulations obtained with the aid of innovative machine learning algorithms and neural networks in order to maintain the highest accuracy level but reduce up to 92% the necessary computational time. The presented methodology would reduce the impact of generating new LFS and ignition delay time correlations when changing fuel or fuel surrogate, thus allowing researchers to investigate more rapidly the impact of these variations.

From the engine simulation point of view, adding water makes the combustion system simulation challenging and the chemistry modeling is asked to be more complex and accurate because of the effect of the water dilution amount on the mixture reactivity. In this case, the proper and detailed evaluation of the chemical properties of the mixture showed to be a key player for addressing the engine designers towards the best solution where the water-cooling effect is balanced by longer combustion duration.

Summarizing the main combustion results:

1. Cases λ 1.0 and λ 0.85 have rapid combustion thanks to the high thermal regime without water dilution and to favorable equivalence ratio, but the thermal regime leads them to detonation or in any case to excessive exhaust temperature if compared to the TiT threshold.
2. PWI cases have higher laminar flame speed than DWI solutions because the water quantity is lower, i.e. s 0.30 vs s 0.35.
3. For DWI s 0.35 p 150 bar IMEPH lies between λ 1.0 - λ 0.85 cases and λ 0.75 case: it does not detonate because the temperature regime is low but not so much to 'cool the flame', as in the case of DWI s 0.55.
4. At CR 9.5, only with λ 0.75 strategy and DWI system s 0.35 150 bar it is possible to reach an exhaust temperature values below the threshold. In case of DWI it is necessary to advance consistently the ignition timing with respect to the case λ 0.75, so accepting combustion efficiency decay.
5. For the same DWI case (s 0.35) but with CR 10.5, apparently it is not possible to drop the temperature below the threshold because of the limited evaporation rate which affects strongly the cooling effect, but it is necessary to keep in mind that these performances are reached with a higher load. Reducing the load, it is admissible to think that this temperature threshold can be reached, also considering the new TiT limits allowed by the upcoming turbocharger technology advancements.
6. DWI system performances are always better than those of PWI system, which represents the least expensive solution and then the research on it should be continued in authors' opinion. The DWI solution, considering these results, is less interesting because it is designed to introduce large quantities of evaporated water into the engine, but at the

expense of the combustion speed. Thus, it is limited by an important intrinsic constraint.

The above reported combustion results have shown that the same IMEPH target is reached for a reduced SA with respect to the solution without water, but the exhaust temperature does not satisfy the constraint of the TiT limit. For reducing the exhaust temperature, it is necessary to increase the SA, with a consequent increase of the engine load. The latter is due the low thermal load (temperature drop) and the dilution effects (water vapor acts as an inert) correlated to the water addition: the water injection slows down the combustion process and thereby the spark timing needs to be advanced for obtaining the target IMEPH but with a reduced quantity of fuel burnt.

References

1. Stefania Falfari, Gian Marco Bianchi, Giulio Cazzoli, Claudio Forte, Sergio Negro, “Basics on Water Injection Process for Gasoline Engines”, Energy Procedia (2018) pp. 50-57 DOI information: 10.1016/j.egypro.2018.08.018.
2. Falfari, S., Bianchi, G.M., Cazzoli, G., Ricci, M. et al., “Water Injection Applicability to Gasoline Engines: Thermodynamic Analysis,” SAE Technical Paper 2019-01-0266, 2019, doi:10.4271/2019-01-0266.
3. Giulio Cazzoli, Gian Marco Bianchi, Stefania Falfari, Claudio Forte, “Development of a chemical-kinetic database for the laminar flame speed under GDI and water injection engine conditions”, Energy Procedia (2018) pp. 154-161 DOI information: 10.1016/j.egypro.2018.08.043.
4. Cazzoli, G., Bianchi, G.M., Falfari, S., Ricci, M. et al., “Evaluation of Water and EGR Effects on Combustion Characteristics of GDI Engines Using a Chemical Kinetics Approach,” SAE Technical Paper 2019-24-0019, 2019, doi:10.4271/2019-24-0019.
5. F. Berni, S. Breda, M. Lugli, G. Cantore, “A numerical investigation on the potentials of water injection to increase knock resistance and reduce fuel consumption in highly downsized GDI engines”, Energy Procedia (2015), pp. 826-835, doi: 10.1016/j.egypro.2015.12.091.
6. d'Adamo, A., Berni, F., Breda, S., Lugli, M. et al., "A Numerical Investigation on the Potentials of Water Injection as a Fuel Efficiency Enhancer in Highly Downsized GDI Engines," SAE Technical Paper 2015-01-0393, 2015, doi:10.4271/2015-01-0393.
7. Battistoni, M., Grimaldi, C., Cruccolini, V., Discepoli, G. et al., “Assessment of Port Water Injection Strategies to Control Knock in a GDI Engine through Multi-Cycle CFD Simulations,” SAE Technical Paper 2017-24-0034, 2017, doi:10.4271/2017-24-0034.
8. Netzer, C., Franken, T., Seidel, L., Lehtiniemi, H. et al., “Numerical Analysis of the Impact of Water Injection on Combustion and Thermodynamics in a Gasoline Engine using Detailed Chemistry,” SAE Technical Paper 2018-01-0200, 2018, doi:10.4271/2018-01-0200.
9. De Bellis, V., Bozza, F., Teodosio, L., and Valentino, G., “Experimental and Numerical Study of the Water Injection to Improve the Fuel Economy of a Small Size Turbocharged SI Engine,” SAE Int. J. Engines 10(2):550-561, 2017, https://doi.org/10.4271/2017-01-0540.
10. Iacobacci, A., Marchitto, L., and Valentino, G., “Water Injection to Enhance Performance and Emissions of a Turbocharged Gasoline Engine under High Load Condition,” SAE Int. J. Engines 10(3):928-937, 2017, https://doi.org/10.4271/2017-01-0660.
11. Pulga, L., Bianchi, G., Ricci, M., Cazzoli, G. et al., “Development of a Novel Machine Learning Methodology for the Generation of a Gasoline Surrogate Laminar Flame Speed Database under Water Injection Engine Conditions,” SAE Int. J. Fuels Lubr. 13(1):2020, doi:10.4271/04-13-01-0001.
12. Raut, A. and Mallikarjuna, J., “Effects of Water Injector Spray Angle and Injector Orientation on Emission and Performance of a GDI Engine—A CFD Analysis,” SAE Int. J. Engines 13(1):17-33, 2020, doi:10.4271/03-13-01-0002.
13. Gern, M. S., Vacca, A., and Bargende, M., “Experimental Analysis of the Influence of Water Injection Strategies on DISI Engine Particle Emissions,” SAE Technical Paper 2019-24-0101, 2019, doi:10.4271/2019-24-0101.
14. Vacca, A., Bargende, M., Chiodi, M., Franken, T. et al., “Analysis of Water Injection Strategies to Exploit the Thermodynamic Effects of Water in Gasoline Engines by Means of a 3D-CFD Virtual Test Bench,” SAE Technical Paper 2019-24-0102, 2019, doi:10.4271/2019-24-0102.
15. Fandakov, A., Grill, M., Bargende, M., and Kulzer, A.C., “A Two-Stage Knock Model for the Development of Future SI Engine Concepts,” SAE Technical Paper 2018-01-0855, 2018, doi:10.4271/2018-01-0855.
16. Fandakov, A., Grill, M., Bargende, M., and Kulzer, A., "Two-Stage Ignition Occurrence in the End Gas and Modeling Its Influence on Engine Knock," SAE Int. J. Engines 10(4):2017, doi:10.4271/2017-24-0001.
17. Poinsot, T., Veynante, D., “Theoretical and Numerical Combustion”, 2001, Edwards, 9781930217058
18. Dekena, M., Peters, N., “Combustion modeling with the G-equation”, Oil Gas Sci. Technol. 54 (1999) 265–270
19. Colin O., Benkenida A. “The 3-Zone Extended Coherent Flame Model (ECFM3Z) for computing premixed/diffusion combustion”, Oil Gas Sci. Technol. -Rev. IFP 59, 6, 593-609.
20. Metghalchi, M., Keck, J., 1982. “Burning velocities of mixtures of air with methanol, isooctane, and indolene at high pressure and temperature”. Combustion and Flame, 48(C), pp. 191-210.
21. Cazzoli, G., Forte, C., Bianchi, G., Falfari, S., Negro, S., "A Chemical-Kinetic Approach to the Definition of the Laminar Flame Speed for the Simulation of the Combustion of Spark-Ignition Engines", SAE Technical Paper 2017-24-0035, 2017, DOI: 10.4271/2017-24-0035.
22. Pulga, L., Bianchi, G.M., Falfari, S. e Forte, C.” A machine learning methodology for improving the accuracy of laminar flame simulations with reduced chemical kinetics mechanisms”, Combustion and Flame, Vol. 216, pp 72-81, https://doi.org/10.1016/j.combustflame.2020.02.021, 2020.
23. Pulga, L., Bianchi, G., Ricci, M., Cazzoli, G. et al., "Development of a Novel Machine Learning Methodology for the Generation of a Gasoline Surrogate Laminar Flame Speed Database under Water Injection Engine Conditions," SAE Int. J. Fuels Lubr. 13(1):5-17, 2020, https://doi.org/10.4271/04-13-01-0001.
24. Lin, H., Zhao, P., and Ge, H., "A Computational Study on Laminar Flame Propagation in Mixtures with Non-Zero Reaction Progress," SAE Technical Paper 2019-01-0946, 2019, https://doi.org/10.4271/2019-01-0946.
25. Van Rossum, G., “Python tutorial”, Technical Report CS-R9526, Centrum voor Wiskunde en Informatica (CWI), Amsterdam, May 1995
26. Cantera: An object-oriented software toolkit for chemical kinetics, thermodynamics, and transport processes. http://www.cantera.org
27. S. Jerzembeck, N. Peters, P. Pepiot-Desjardins, H. Pitsch, “Laminar burning velocities at high pressure for primary reference fuels and gasoline: Experimental and numerical

investigation", Combustion and Flame, Volume 156, Issue 2, 2009, Pages 292-301, ISSN 0010-2180, DOI:10.1016/j.combustflame.2008.11.009
28. Ranzi, E., Frassoldati, A., Stagni, A., Pelucchi, M., Cuoci, A., Faravelli, T., "Reduced kinetic schemes of complex reaction systems: Fossil and biomass-derived transportation fuels", International Journal of Chemical Kinetics, 46 (9), pp. 512-542 (2014), DOI:10.1002/kin.20867
29. Kyle E. Niemeyer and Chih-Jen Sung. On the importance of graph search algorithms for DRGEP-based mechanism reduction methods. *Combustion and Flame*, 158(8):1439–1443, 2011. doi: 10.1016/j.combustflame.2010.12.010.
30. Kyle E. Niemeyer, Chih-Jen Sung, and Mandhapati P. Raju. Skeletal mechanism generation for surrogate fuels using directed relation graph with error propagation and sensitivity analysis. *Combustion and Flame*, 157(9):1760–1770, 2010. doi: 10.1016/j.combustflame.2009.12.022.
31. P. O. Mestas, P. Clayton, and K. E. Niemeyer. (2019) pyMARS v1.1.0 [software]. Zenodo. https://doi.org/10.5281/zenodo.3401549
32. Zhu, J., Zou, H., Rosset, S., Hastie, T., "Multi-class AdaBoost", 2009.
33. Pedregosa, F., Varoquaux, G., Gramfort, A., Michel, V., Thirion, B., Grisel, O., et al., "Scikit-Learn: Machine Learning in Python", Journal of Machine Learning Research, Vol. 12, pp. 2825-2830, 2011
34. Chollet, F., et al.., Keras, 2015, https://keras.io
35. Del Pecchia, M., Breda, S., D'Adamo, A., Fontanesi, S. et al., "Development of Chemistry-Based Laminar Flame Speed Correlation for Part-Load SI Conditions and Validation in a GDI Research Engine", SAE Int. J. Engines 11(6):715-741, 2018, DOI: 10.4271/2018-01-0174
36. B.M. Gauthier, D.F. Davidson, R.K. Hanson, Shock tube determination of ignition delay times in full-blend and surrogate fuel mixtures, Combustion and Flame, Volume 139, Issue 4, 2004, Pages 300-311, ISSN 0010-2180, https://doi.org/10.1016/j.combustflame.2004.08.015.
37. Siokos, K., He, Z., and Prucka, R., "Assessment of Model-Based Knock Prediction Methods for Spark-Ignition Engines," SAE Technical Paper 2017-01-0791, 2017, https://doi-org.ezproxy.unibo.it/10.4271/2017-01-0791.
38. Forte, C., Corti, E., Bianchi, G., Falfari, S. et al., "A RANS CFD 3D Methodology for the Evaluation of the Effects of Cycle By Cycle Variation on Knock Tendency of a High Performance Spark Ignition Engine," SAE Technical Paper 2014-01-1223, 2014, doi:10.4271/2014-01-1223.

Contact Information

For further information/details please contact:

leonardo.pulga2@unibo.it